Interference of a Bose-Einstein condensate in a hard-wall trap: From the nonlinear Talbot effect to the formation of vorticity

J. Ruostekoski,[1,2] B. Kneer,[2] W. P. Schleich,[2] and G. Rempe[3]
[1]*Department of Physical Sciences, University of Hertfordshire, Hatfield, Hertfordshire AL10 9AB, United Kingdom*
[2]*Abteilung für Quantenphysik, Universität Ulm, D-89069 Ulm, Germany*
[3]*Max-Planck-Institut für Quantenoptik, Hans-Kopfermann-Strasse 1, D-85748 Garching, Germany*
(Received 2 August 1999; revised manuscript received 20 December 2000; published 20 March 2001)

We theoretically study the coherent expansion of a Bose-Einstein condensate in the presence of a confining impenetrable hard-wall potential. The nonlinear dynamics of the macroscopically coherent matter field results in rich and complex spatiotemporal self-interference patterns demonstrating a nonlinear Talbot effect, and the formation of vorticity and solitonlike structures.

DOI: 10.1103/PhysRevA.63.043613 PACS number(s): 03.75.Fi, 05.30.Jp

I. INTRODUCTION

A landmark experiment [1] demonstrated in a striking way the interference of two freely expanding Bose-Einstein condensates (BECs). In this paper we theoretically study the evolution of a BEC in a coherently reflecting hard-wall trap. The hard-wall boundary conditions allow us to investigate a nonlinear matter-wave Talbot effect, which has been recently demonstrated for BECs in a linear regime by means of an electromagnetic pulsed grating [2]. The present situation is also closely related to the recent experiments on a BEC bouncing off a mirror [3,4] and on an expanding condensate in an optically-induced ''box'' potential [5,6]. Due to the macroscopic quantum coherence, the BEC exhibits rich and complex self-interference patterns. We identify the formation of vorticity and solitonlike structures, and the fragmentation of an initially uniform parabolic BEC into coherently coupled pieces.

Atomic BECs exhibit a macroscopic quantum coherence in analogy to the optical coherence of lasers. In the conventional reasoning, the coherence of a BEC is introduced in the spontaneous symmetry breaking. Nevertheless, even two BECs with no phase information could show relative phase correlations as a result of the back action of quantum measurement [7]. Moreover, the density-dependent self-interaction of a BEC demonstrates the analogy between nonlinear laser optics and *nonlinear atom optics* [8,9] with BECs. BECs are predicted to exhibit dramatic coherence properties: The macroscopic coherent quantum tunneling [10] and the formation of fundamental structures; e.g., vortices [11–15] and solitons [16,17,8,18]. Some basic properties of gray solitons have been recently addressed for harmonically trapped one-dimensional (1D) BECs in Ref. [18]. Also, optical solitons have been actively studied in the 1D homogeneous space [19].

This paper is organized as follows: In Sec. II we introduce the basic setup of the self-interference study. The nonlinear Talbot effect of a BEC in a 1D box is considered in Sec. III. The evolution of a BEC in a 1D box demonstrates the macroscopic matter wave coherence and the formation of solitonlike structures in Sec. III A. In Sec. III B we show that similar structures may also be observable in an experimentally realized 3D trap configuration [20,21]. The evolution of a BEC in 2D hard-wall traps is considered in Sec. IV. For a disk with a rotationally symmetric initial state, we again identify the solitonlike structures in Sec. IV A. When the rotational symmetry of the initial state is broken, we show in Sec. IV B that the structures bend and break up forming vorticity. A square box is studied in Sec. IV C. Finally, a few concluding remarks are made in Sec. V.

II. FORMULATION OF THE PROBLEM

In this section we introduce the basic setup and the theoretical model of matter-wave self-interference resulting from the expansion and the reflection of a BEC.

A. A hard-wall trap

We study the dynamics of a BEC confined to a hard-wall trap with potential $V(\mathbf{r})$. Such walls can be realized, e.g., optically with a blue-detuned far-off-resonant light sheet. A higher-order Laguerre-Gaussian beam can generate a hollow optical beam [22] and thus a cylindrical atom-optical hard-wall potential around the magnetically trapped BEC. Recent experiments [3–5] considered the coherent reflections of a BEC by atom-optical mirrors and the evolution of a BEC in an atom-optical waveguide closely related to the present theoretical study. The evolution of a BEC in a 1D box potential also represents a nonlinear analogue of the electromagnetic pulsed-grating Talbot effect [2], in which case pulsed lasers generate copies of BECs in momentum space similarly to the 1D box potential. Due to the strong nonlinearity, the dispersion relation of atoms in the hard-wall potential becomes nonquadratic.

B. Self-interference

Throughout the paper we focus on repulsive interactions. When the BEC is released from a magnetic trap, the repulsive mean-field energy of the condensate transforms into kinetic energy and the BEC rapidly expands towards the walls. The reflections of the matter wave from the binding potential result in rich and complex spatiotemporal interference patterns referred to in 1D as quantum carpets [23]. Nonlinear self-interference in a 1D box has been investigated in Refs.

[3,5,6]. Moreover, a thermometer for measuring the temperature of the BEC based on this effect is also proposed [24].

In this paper we study the nonlinear Talbot effect of a coherent matter field. This effect is analogous to the near-field optical Fresnel diffraction. Here the periodicity of the grating in the optical Talbot effect is represented by the reflecting hard-wall boundaries confining the BEC. The nonlinearity of the Talbot effect and the strong self-interaction of the matter field result from the confinement. We show that a BEC displays complex nonlinear self-interference dynamics including the formation of solitonlike structures and vorticity. The solitary waves could possibly be used as an experimental realization of the macroscopic coherent tunneling analogous to the Josephson effect.

The density profiles of the BECs could be directly measured via absorption imaging, if the necessary spatial resolution could be obtained, e.g., via ballistic expansion of the atomic cloud. Vortices may also be detected by interfering a BEC with and without vorticity. Then the phase slip in the interference fringes would be the signature of the vorticity [11,15]. The phase slip between two pieces of the BEC has a dramatic effect on the dynamical structure factor of the two-component system [25] that may be observed, e.g., via the Bragg scattering [26]. However, we note that the dynamics of the matter field may complicate interference experiments.

C. Theoretical model

The dynamics of a BEC follows from the Gross-Pitaevskii equation (GPE)

$$i\hbar\frac{\partial}{\partial t}\psi(\mathbf{r};t)=\left[-\frac{\hbar^2}{2M}\nabla^2+V(\mathbf{r})+\kappa|\psi(\mathbf{r};t)|^2\right]\psi(\mathbf{r};t).$$

Here M and $\kappa\equiv 4\pi\hbar^2 aN/M$ denote the atomic mass and the coefficient of the nonlinearity, respectively, with the scattering length a and the number N of BEC atoms. Our initial distribution $\psi(\mathbf{r};t=0)$ is the stationary solution of the GPE with the potential $V(\mathbf{r})$ replaced by the potential of the magnetic trap.

We integrate GPE in one, two, and three spatial dimensions. The projections from 3D into 1D or 2D require that the mean field ψ does not vary significantly as a function of time in the corresponding orthogonal directions. This condition can be satisfied, e.g., in the presence of a strong spatial confinement to these dimensions. Then we can approximate the position dependence in these directions by constants $\mathcal{A}$ and ℓ resulting in $\psi(\mathbf{r})\simeq\psi_1(x)/\mathcal{A}^{1/2}$ in 1D and $\psi(\mathbf{r})\simeq\psi_2(x,y)/\ell^{1/2}$ in 2D. This yields the strengths $\kappa_1\simeq\kappa/\mathcal{A}$ and $\kappa_2\simeq\kappa/\ell$ of the nonlinearity in the GPE for the mean fields in 1D and 2D, ψ_1 and ψ_2. We emphasize that in the present problem especially the 2D calculations may already contain the essential features of the full 3D coupling between the different spatial dimensions by the nonlinearity.

We explicitly demonstrate how the solitonlike structures obtained in a 1D trap may also be observed in an anisotropic 3D magnetic trap configuration [20,21]. Moreover, the 1D and 2D calculations may be directly applicable to atom traps with strong spatial confinement in orthogonal dimensions.

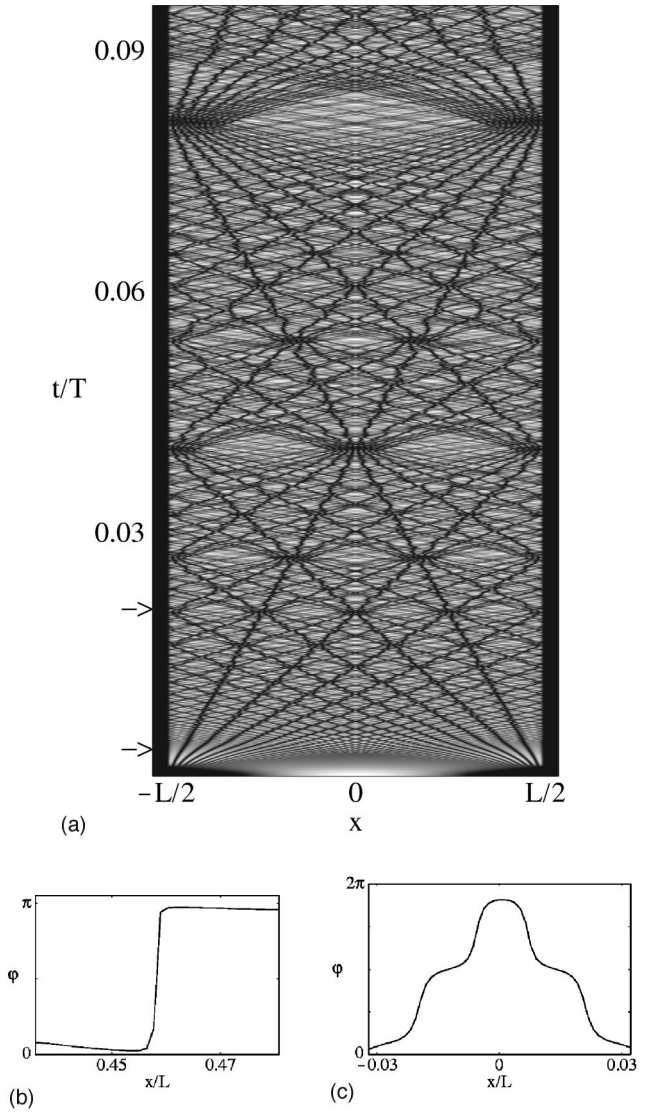

FIG. 1. A nonlinear Talbot effect in a BEC with propagating gray solitonlike structures. Time evolution (a) of a BEC density profile $|\psi_1(x;t)|^2$ in a 1D hard-wall trap. The horizontal and vertical axes denote the spatial coordinate and time, respectively. The initially confined BEC expands towards, and reflects from, the hard-wall boundaries. The dark canals correspond to low density and represent the evolution of gray solitonlike structures. The phase slip of a single fringe (b) at $t/T\simeq 3.2\times 10^{-3}$, and of four colliding fringes (c) at $t/T\simeq 0.021$. The arrows in (a) denote the times of the phase profiles (b) and (c). Here the initial state is $R/L\simeq 0.3$ and $\kappa_1=19\,000L\hbar/T$.

We assume that the density fluctuations in these orthogonal dimensions are negligible, but we do not consider the limit where the atoms in the trap become impenetrable [27]. In this case, we can translate the nonlinearities used in 1D and 2D into the parameters describing the trap geometry and the number of atoms. For example, in Fig. 1 we use the nonlinearity $\kappa_1=19\,000L\hbar/T$. For ^{87}Rb atoms stored in a tightly confined quasi-1D trap with the effective radial extension of the wave function $\mathcal{A}=(0.5\ \mu\mathrm{m})^2$, the box length $L=15\ \mu$m, and with the s-wave scattering length a

$=5.4$ nm, this value of κ_1 corresponds to $N \simeq 4000$. Similarly, in Figs. 3 and 4 we have $\kappa_2 \equiv 1500\hbar^2/M$, which with the spatial confinement constant $\ell = 0.5$ μm corresponds approximately to 11 000 atoms. For the same geometry the value $\kappa_2 \equiv 5000\hbar^2/M$ in Fig. 6 represents about 38 000 atoms.

III. NONLINEAR TALBOT EFFECT

In this section we study the nonlinear Talbot effect of a BEC in a 1D box and the emergence of spatiotemporal solitonlike structures. We demonstrate that similar structures may also be observed in an experimentally realized 3D magnetic trap [20,21].

A. One-dimensional trap

The linear Schrödinger equation for the 1D box of length L exhibits [23] regular spatiotemporal patterns. These patterns consist of straight lines, so-called traces, of different steepness corresponding to harmonics of a fundamental velocity v_0. The traces arise from the interferences between degenerate eigenmodes of the system. The eigenmodes of frequency $\omega_n \equiv n^2\omega_1 \equiv n^2\hbar\pi^2/(2ML^2)$ are a superposition of right and left propagating plane waves with wave numbers $k_n \equiv n\pi/L \equiv nk_1$. The probability density consists of the interferences between different eigenmodes. Therefore, the lines of constant phase $\pm(k_m \pm k_n)x + (\omega_m - \omega_n)t = \text{const.}$ correspond to straight lines in space-time with velocities $v_{mn} \equiv \pm(\omega_m - \omega_n)/(k_m \pm k_n) = (m \pm n)v_0$. Here we introduced the fundamental trace velocity $v_0 \equiv \hbar\pi/(2mL)$.

The wave function of the linear Schrödinger equation is temporally reconstructed at multiples of the Talbot time $T \equiv 2\pi/\omega_1 \equiv 4ML^2/(\pi\hbar)$. The revival time for the density profile with a symmetric initial state is $T/8$. In addition, at the rational fractions of the Talbot time, modified images of the wave function are produced.

We now turn to the nonlinear Talbot effect of Fig. 1(a), representing a 1D BEC trapped between two impenetrable steep Gaussian potentials

$$V(x) = \mathcal{A}[g(x - \tilde{L}/2) + g(x + \tilde{L}/2)],$$

where we have defined

$$g(x) \equiv \exp\left[-\left(\frac{x}{L\alpha}\right)^2\right], \quad \tilde{L} \equiv (1+\eta)L.$$

We use the height $\mathcal{A} = 10^{15}\hbar^2/(ML^2)$ and the width $\alpha = 0.01$. The parameter $\eta \simeq 0.10$ is chosen in such a way that the potential approximates infinitely high walls located at $x = \pm L/2$.

At time $t = 0$, the BEC is released from a harmonic trap of frequency Ω. In the limit of strong confinement, the mean-field self-energy dominates the kinetic energy and the initial state is well approximated by the Thomas-Fermi solution $\psi_1(x; t=0) = \theta(R_1 - |x|)[3(R_1^2 - x^2)/(2R_1^3)]^{1/2}$. Here $R_1 \equiv [3\kappa_1/(M\Omega^2)]^{1/3}$ describes the 1D radius of the BEC wave function.

After the turnoff of the magnetic trap, the kinetic energy term in the GPE becomes dominant and the matter wave expands towards, and eventually reflects from, the box boundaries. Due to the macroscopic quantum coherence of a BEC, different spatial regions of the matter field generate a complex self-interference pattern that exhibits canals analogous to the quantum carpet structures of the linear Schrödinger equation [23]. From Fig. 1 we note that only destructive interference fringes, canals, appear in the nonlinear carpet. Constructive interference fringes, ridges, do not emerge. The convergence of the numerical integration is checked by varying the size of the time step and the number of spatial grid points.

1. Solitonlike behavior

For the single-particle Schrödinger equation, the resulting interference pattern demonstrates the fundamental *wave nature* of the particle. Therefore, it is perhaps surprising that in the case of the GPE, which represents the coherent matter *field* of the many-particle system, the intermode traces acquire properties that demonstrate *particle nature*. In particular, in the case of repulsive interparticle interactions, the traces correspond to the evolution of solitonlike structures [19,18].

Gray solitons correspond to the propagation of ''density holes'' in the matter field and the depth of the hole characterizes the grayness of the soliton. In homogeneous space the soliton is called dark when it exhibits [19,18] a vanishing density at the center of the dip and a sharp phase slip of π. For gray solitons the value of the phase slip φ is reduced, thereby giving the soliton a nonvanishing speed according to $v = c\cos(\varphi/2)$, where the maximum velocity $c \equiv (4\pi\hbar^2 a\rho/M^2)^{1/2}$ is the Bogoliubov speed of sound at a constant atom density ρ. As a result of the formation of the solitonlike structures, the initially uniform parabolic BEC is fragmented into spatially separated pieces and we can interpret these density holes as the boundaries of the fragmented BEC. Analogous to the Josephson junction, the phase of the BEC is approximately constant outside the narrow region of the solitary wave [18]. The coherent tunneling of atoms across the boundary depends on the relative phase between the two contiguous pieces and results in the motion of the ''solitary wave junction.'' For a phase slip of π, the velocity of the soliton vanishes analogously to the vanishing Josephson oscillations of the number of atoms.

The interatomic interactions shift the eigenenergies compared to the linear case and the dispersion relation of atoms is nonquadratic. As a result, the fringe velocities in Fig. 1 are a few tens of percents larger than the linear trace velocities $4nv_0$ for the canals with a symmetric initial state [23] and we do not observe a complete revival of the wave packet as in the case of a linear Talbot effect [2]. The nonlinear fringe velocities are still determined by the degenerate intermode traces and are approximately integer multiples of the minimum speed. The largest velocity in Fig. 1 is approximately given by the Bogoliubov speed of sound in terms of the average density of atoms in the box.

The fringe evolution shown in Fig. 1 displays a remarkable inherent particlelike robustness and solitonlike behavior: The fringes survive complex dynamics. Their paths ex-

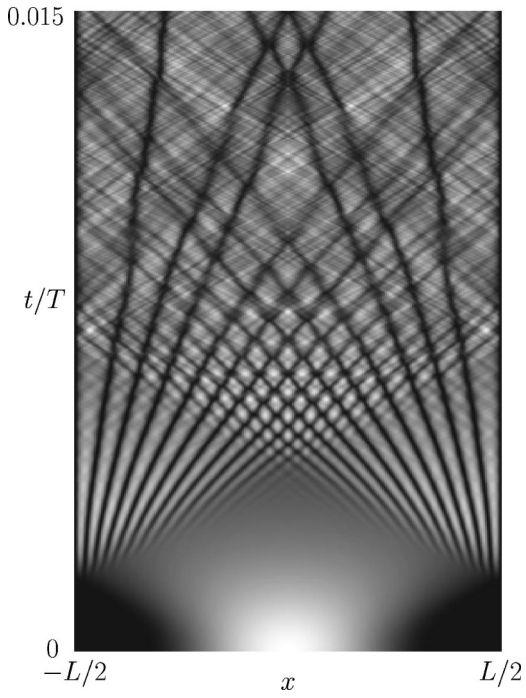

FIG. 2. A 1D axial projection of an expanding BEC in a cylindrical 3D trap. We show the time evolution of a BEC density profile $|\bar{\psi}(x;t)|^2=\int dy\, dz|\psi(\mathbf{r};t)|^2$. The horizontal and vertical axes denote the axial coordinate x and time t, respectively. We have integrated over the atom density in the radial direction. The initially confined BEC expands axially towards, and reflects from, the hard-wall boundaries, while still harmonically confined in the radial direction. The dark canals correspond to low density and represent the evolution of gray solitonlike structures.

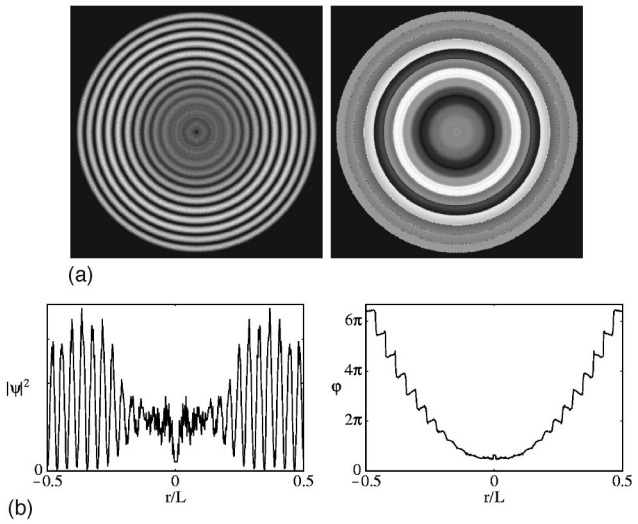

FIG. 3. Formation of loops of solitonlike structures in a BEC expanding in a 2D circular box. The symmetric condensate has started from the center of the circular box, has expanded and reflected from the boundary. We show (a) the density (left) and phase (right) profiles of the BEC at time $t=4.9\times10^{-3}ML^2/\hbar$. In the phase profile we have chosen a continuous phase $|\varphi|$, where $-\pi\leqslant\varphi\leqslant\pi$. The corresponding (b) 1D radial cuts of the rotationally symmetric density (left) and phase φ (right). The initial state is $R_2/L\simeq0.28$ and $\kappa_2\equiv1500\hbar^2/M$.

hibit dramatic avoided crossings demonstrating repulsive interactions. The repulsive interactions in coordinate space correspond to attractive interactions in momentum space and the avoided crossings represent the degeneracy of the colliding wave-packet holes in momentum space [28].

B. Three-dimensional trap

Motivated by the 1D calculations presented in Fig. 1, we investigate whether the 1D structures can also be observable in 3D trap configurations. We consider a ''cigar-shaped'' and highly anisotropic, but still a 3D trap used in Refs. [20,21]. In Refs. [20,21] ^{87}Rb atoms are trapped in a dc magnetic field generated by currents through a cliplike coil for radial confinement and two pinch coils for axial confinement. The atoms can be released along the axial direction, while still confined in the radial direction by the magnetic fields. Blue-detuned laser sheets can introduce the hard-wall potential in the axial direction.

The initial state is a ^{87}Rb BEC with 10 000 atoms confined in a magnetic trap with the trapping frequencies in the axial and radial directions $\Omega_x\simeq2\pi\times25$ Hz and $\Omega_\perp\simeq2\pi\times250$ Hz, respectively [21]. For ^{87}Rb we use the s-wave scattering length $a=5.4$ nm. At time $t=0$, the atoms are released along the axial direction by setting $\Omega_x=0$. The BEC expands and reflects from the laser sheets located at $x=\pm L/2$. The Thomas-Fermi radius of the initial state in the axial direction $R_x\equiv[15\kappa\lambda^4/(4\pi M\Omega_\perp^2)]^{1/5}$ satisfies $R_x/L\simeq0.33$. Here we have defined $\lambda\equiv\Omega_\perp/\Omega_x$. We assume that the density profile of the atoms is measured in the xy plane; e.g., by means of an absorption imaging. Furthermore, we assume that the obtained signal is also integrated along the y axis resulting in a 1D density profile that only depends on the axial coordinate x:

$$|\bar{\psi}(x;t)|^2\equiv\int dy\, dz|\psi(\mathbf{r};t)|^2=2\pi\int d\rho\rho|\psi(x,\rho;t)|^2.$$

Here we have introduced $\rho\equiv(y^2+z^2)^{1/2}$.

We solve the 3D GPE in the cylindrically symmetric configuration by expanding the wave function along ρ in the 2D harmonic oscillator basis set. In the calculated 3D density profile, we integrate over ρ. Figure 2 shows the resulting 1D atom density time evolution. We note the similar solitonlike structures as obtained in the 1D trap displayed in Fig. 1. Some of the structures are vanishing, corresponding to the instability of solitons in 3D [19]. The similarity between the 1D and 3D solutions in Figs. 1 and 2 is significant considering that the present 3D trap does not confine the atoms very strongly in the radial direction. We also note differences between the two situations: In the 3D case, the evolution of the wave-packet holes is slightly curved even if the wave packets are not close to each other. In the 1D projection of the 3D dynamics, the repulsion between the solitonlike structures is also not as clearly displayed as in the 1D case.

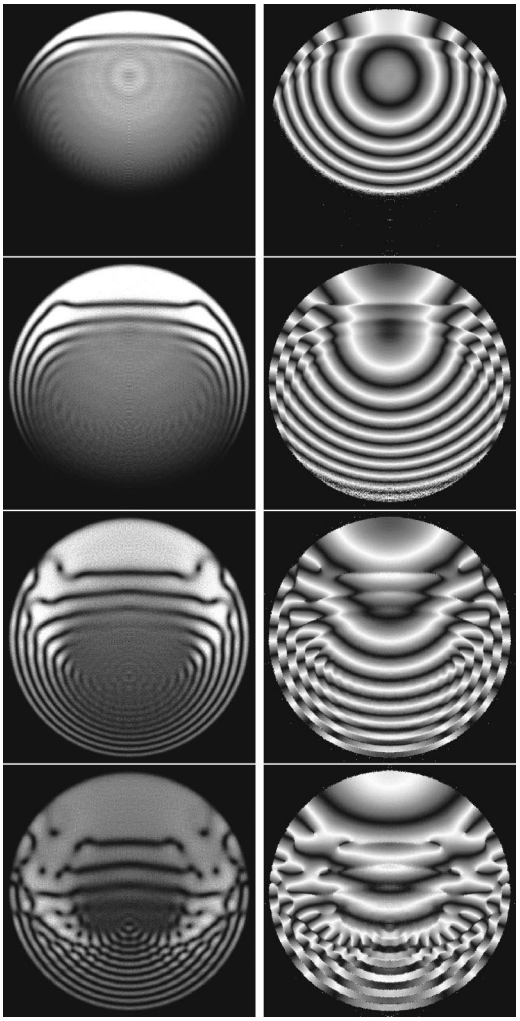

FIG. 4. Formation of vorticity in a BEC expanding in a 2D circular box with displaced initial state. We show the density profiles (left column) and the corresponding phase profiles (right column) of the BEC at four characteristic times $t=2.5\times10^{-3}$, $t=3.7\times10^{-3}$, 4.9×10^{-3}, and 6.1×10^{-3} in units of $ML^2/\hbar$. The reflections from the boundary generate solitonlike structures that bend, break up, and form vorticity. The velocity of the BEC is proportional to the gradient of the phase.

IV. SELF-INTERFERENCE IN TWO DIMENSIONS

In the previous section we studied the 1D spatial structures in the nonlinear Talbot effect by simulating the expansion of a BEC in 1D and 3D hard-wall traps. In this section we consider higher dimensional self-interference structures of a BEC. In particular, we study 2D structures formed in 2D hard-wall traps. We consider a circular disk and a square box. When the rotational symmetry of the initial state is broken, solitonlike structures bend and break up forming vorticity.

A. A disk with a symmetric initial state

We now turn to the evolution of a BEC in a circular box. Again we approximate the infinitely high walls by a steep Gaussian potential aligned along a circle of radius $r\equiv L/2$.

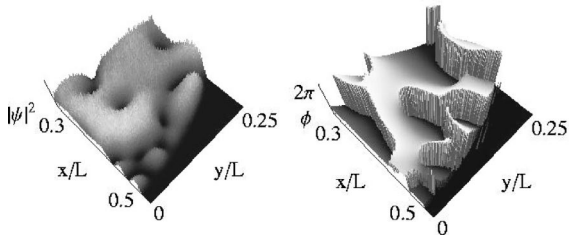

FIG. 5. The 3D magnification of the density and the phase φ from the upper right corner of the last density and phase profile of Fig. 4 displaying vorticity. For example, the dark spot in the center represents a vortex with a unit circular quantization of 2π.

The parameters $\mathcal{A}$, α, and η are the same as in the 1D case. The initial wave function is the Thomas-Fermi solution of the isotropic trap $\psi_2(x,y;t=0)=\theta(R_2^2-x^2-y^2)[2(R_2^2-x^2-y^2)/(\pi R_2^4)]^{1/2}$, and $R_2\equiv[4\kappa_2/(\pi M\Omega^2)]^{1/4}$ denotes the 2D Thomas-Fermi radius. Hence, the initial wave function is located at the center of the circular box and we can show that in this case the state remains symmetric also at later times.

Figure 3 shows the 2D density $|\psi_2(x,y;t)|^2$ and the phase profile $|\varphi|$ of a BEC obtained from the GPE at a later time, representing a snapshot of the evolving matter field. We note the formation of a regular interference pattern outside the central region of the trap similar to solitary waves. The fragmentation of the BEC is more dramatic than in the 1D case: The fringes exhibit a vanishing density at the center of the dip. The BEC forms coherently coupled loops and the resulting structures are similar to optical ring solitons [19].

B. A disk with an asymmetric initial state

When we now slightly displace the initial state of the BEC from the center of the circular box, the rotational symmetry is broken. In Figs. 4 and 5 we show the resulting 2D density (left column) and the phase profiles (right column) at four characteristic times. The reflections of the coherent matter wave from the hard-wall potential create solitonlike structures. At later times, the stripes bend and eventually break

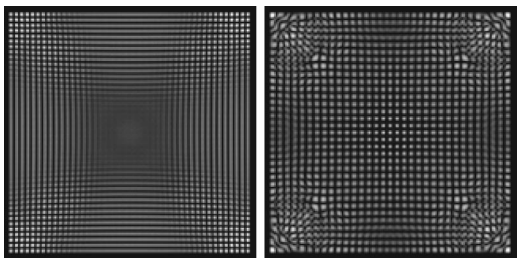

FIG. 6. Expanding BEC in a 2D square box with a symmetric initial state at the center of the square. At $t=2.9\times10^{-3}ML^2/\hbar$ (left) the density profile of the BEC exhibits a rectangular pattern of solitonlike structures. At a later time $t=3.9\times10^{-3}ML^2/\hbar$ (right), the pattern is distorted and we see the beginning of the formation of vorticity symmetrically around the diagonals. The initial radius of the BEC is $R_2/L\simeq0.28$ and as a representative nonlinearity we have chosen $\kappa_2=5000\hbar^2/M$.

up, forming dark spots that correspond to vortices with associated phase windings around closed paths [13].

We note that we can use the present situation of an expanding BEC in a circular box to create vortices in some particular spatial location by simply introducing a *static* potential dip and letting the expanding BEC flow across it. This is a simplified version of the suggestion by Ref. [14] that a moving potential barrier through a BEC can create vorticity in the vicinity of the potential.

C. A square box

As a final example and to demonstrate the effect of the symmetry of the hard-wall trap, we consider the evolution of a BEC in the 2D square box. We generate the boundary by steep Gaussians approximating infinitely high walls at $x = \pm L/2$ and $y = \pm L/2$.

The square has the symmetry of rotations of $\pi/2$. Hence, for a symmetric nonrotating initial state, the minimum number of vortices conserving the total angular momentum is eight. In Fig. 6 we show the density profile at two characteristic times. The reflections of the BEC from the boundary generate dark solitonlike structures with an amazingly regular square shape that start bending, break up, and form vorticity.

V. CONCLUSIONS

We studied the nonlinear Talbot effect of a macroscopically coherent BEC. The large nonlinearity is possibly due to the confining hard-wall potential resulting in a strong density-dependent self-interaction. The matter-wave Talbot effect is analogous to the optical near-field diffraction Talbot effect: The periodic grating in the optical Talbot effect is represented here by the reflecting hard-wall boundaries. We demonstrated the complex self-interference dynamics of a BEC in a hard-wall trap including the formation of vorticity and solitonlike structures. The nonlinear evolution of the GPE divides the initially uniform parabolic BEC into coherently coupled pieces. We showed that the density profile of the BEC can be a direct manifestation of the macroscopic quantum coherence. Obviously, it could also be a sensitive measure for the decoherence rate of the BEC [29]. Unlike the typical coherence measurement that detects the relative macroscopic phase between two well-distinguishable BECs [1,29], the present setup probes the self-interference of an initially uniform matter field.

ACKNOWLEDGMENTS

We acknowledge financial support from EPSRC, DFG through the Research Consortium in quantum gases, and from the EC through the TMR Network ERBFMRXCT96-0066.

[1] M.R. Andrews, C.G. Townsend, H.-J. Miesner, D.S. Durfee, D.M. Kurn, and W. Ketterle, Science **275**, 637 (1997).
[2] L. Deng, E.W. Hagley, J. Denschlag, J.E. Simsarian, M. Edwards, C.W. Clark, K. Helmerson, S.L. Rolston, and W.D. Phillips, Phys. Rev. Lett. **83**, 5407 (1999).
[3] K. Bongs, S. Burger, G. Birkl, K. Sengstock, W. Ertmer, K. Rzazewski, A. Sanpera, and M. Lewenstein, Phys. Rev. Lett. **83**, 3577 (1999).
[4] M. Boshier *et al.* (unpublished).
[5] S. Burger, K. Bongs, K. Sengstock, and W. Ertmer (unpublished).
[6] For theory, see also P. Villain and M. Lewenstein, Phys. Rev. A **62**, 043601 (2000).
[7] J. Javanainen and S.M. Yoo, Phys. Rev. Lett. **76**, 161 (1996); S.M. Yoo, J. Ruostekoski, and J. Javanainen, J. Mod. Opt. **44**, 1763 (1997).
[8] G. Lenz, P. Meystre, and E.M. Wright, Phys. Rev. Lett. **71**, 3271 (1993).
[9] L. Deng, E. Hagley, J. Wen, M. Trippenbach, Y. Band, P. Julienne, J. Simsarian, K. Helmerson, S. Rolston, and W. Phillips, Nature (London) **398**, 218 (1999).
[10] J. Javanainen, Phys. Rev. Lett. **57**, 3164 (1986); A. Smerzi, S. Fantoni, S. Giovanazzi, and S. R. Shenoy, *ibid.* **79**, 4950 (1997); J Ruostekoski and D.F. Walls, Phys. Rev. A **58**, R50 (1998); M.W. Jack, M.J. Collett, and D.F. Walls, *ibid.* **54**, R4625 (1996); I. Zapata, A. Leggett, F. Sols, *ibid.* **57**, R28 (1998); J. Williams, R. Walser, J. Cooper, E. Cornell, and M. Holland, *ibid.* **59**, R31 (1999).
[11] M.R. Matthews, B.P. Anderson, P.C. Haljan, D.S. Hall, C.E. Wieman, and E.A. Cornell, Phys. Rev. Lett. **83**, 2498 (1999).
[12] K. Madison, F. Chevy, W. Wohlleben, and J. Dalibard, Phys. Rev. Lett. **84**, 806 (2000).
[13] For recent theoretical studies of the ground-state properties and the stability of vortices in harmonic and toroidal traps: F. Dalfovo and S. Stringari, Phys. Rev. A **53**, 2477 (1996).
[14] B. Jackson, J.F. McCann, and C.S. Adams, Phys. Rev. Lett. **80**, 3903 (1998).
[15] E.L. Bolda and D.F. Walls, Phys. Rev. Lett. **81**, 5477 (1998).
[16] S. Burger, K. Bongs, S. Dettmer, W. Ertmer, K. Sengstock, A. Sanpera, G.V. Shlyapnikov, and M. Lewenstein, Phys. Rev. Lett. **83**, 5198 (1999).
[17] J. Denschlag, J.E. Simsarian, D.L. Feder, C. Clark, L.A. Collins, J. Cubizolles, L. Deng, E.W. Hagley, K. Helmerson, W.P. Reinhard, S.L. Rolston, B.I. Schneider, and W.P. Phillips, Science **287**, 97 (2000).
[18] W.P. Reinhardt and C.W. Clark, J. Phys. B **30**, 785 (1997); T.F. Scott, R.J. Ballagh, and K. Burnett, *ibid.* **31**, 329 (1998); Th. Busch and J.R. Anglin, e-print cond-mat/9809408.
[19] Y.S. Kivshar and B. Luther-Davies, Phys. Rep. **298**, 81 (1998), and references therein.
[20] U. Ernst, A. Marte, F. Schreck, J. Schuster, and G. Rempe, Europhys. Lett. **41**, 1 (1998).
[21] U. Ernst, J. Schuster, F. Schreck, A. Marte, A. Kuhn, and G. Rempe, Appl. Phys. B: Lasers Opt. **67**, 719 (1998).
[22] I. Manek, Yu. B. Ovchinnikov, and R. Grimm, Opt. Commun. **147**, 67 (1998).
[23] A.E. Kaplan, P. Stifter, K.A.H. van Leeuwen, W.E. Lamb, Jr.,

and W.P. Schleich, Phys. Scr. **T76**, 93 (1998); I. Marzoli, F. Saif, I. Bialynicki-Birula, O.M. Friesch, A.E. Kaplan, and W.P. Schleich, Acta Phys. Slov. **48**, 323 (1998).

[24] S. Choi, K. Burnett, O. Friesch, B. Kneer, and W.P. Schleich (unpublished).

[25] J. Ruostekoski and D.F. Walls, Phys. Rev. A **55**, 3625 (1997).

[26] D.M. Stamper-Kurn, A.P. Chikkatur, A. Görlitz, S. Innouye, S. Gupta, D.E. Pritchard, and W. Ketterle, Phys. Rev. Lett. **83**, 2876 (1999).

[27] A.G. Rojo, J.L. Cohen, and P.R. Berman, Phys. Rev. A **60**, 1482 (1999).

[28] The dynamics of the GPE with attractive interactions generates bright solitons consisting of matter-wave packets. However, for large attractive interactions, the BEC remains focused in the center of the trap and the box boundary does not play an important role.

[29] D.S. Hall, M.R. Matthews, C.E. Wieman, and E.A. Cornell, Phys. Rev. Lett. **81**, 1543 (1998).